

# Journal of Biomedical Optics

[SPIEDigitalLibrary.org/jbo](http://SPIEDigitalLibrary.org/jbo)

## **Exploring Raman spectroscopy for the evaluation of glaucomatous retinal changes**

Qi Wang  
Sinisa D. Grozdanic  
Matthew M. Harper  
Nicolas Hamouche  
Helga Kecova  
Tatjana Lazic  
Chenxu Yu

# Exploring Raman spectroscopy for the evaluation of glaucomatous retinal changes

Qi Wang,<sup>a</sup> Sinisa D. Grozdanic,<sup>b</sup> Matthew M. Harper,<sup>b</sup> Nicolas Hamouche,<sup>c</sup> Helga Kecova,<sup>b</sup> Tatjana Lazic,<sup>b</sup> and Chenxu Yu<sup>a</sup>

<sup>a</sup>Iowa State University, Department of Agricultural and Biosystems Engineering, Ames, Iowa 50011

<sup>b</sup>U.S. Department of Veterans Affairs Center for Prevention and Treatment of Visual Loss, 601 HWY 6 West, Iowa City, Iowa, 52246

<sup>c</sup>McFarland Clinic Eye Center, 1128 Duff Avenue, Ames, Iowa 50011

**Abstract.** Glaucoma is a chronic neurodegenerative disease characterized by apoptosis of retinal ganglion cells and subsequent loss of visual function. Early detection of glaucoma is critical for the prevention of permanent structural damage and irreversible vision loss. Raman spectroscopy is a technique that provides rapid biochemical characterization of tissues in a nondestructive and noninvasive fashion. In this study, we explored the potential of using Raman spectroscopy for detection of glaucomatous changes *in vitro*. Raman spectroscopic imaging was conducted on retinal tissues of dogs with hereditary glaucoma and healthy control dogs. The Raman spectra were subjected to multivariate discriminant analysis with a support vector machine algorithm, and a classification model was developed to differentiate disease tissues versus healthy tissues. Spectroscopic analysis of 105 retinal ganglion cells (RGCs) from glaucomatous dogs and 267 RGCs from healthy dogs revealed spectroscopic markers that differentiated glaucomatous specimens from healthy controls. Furthermore, the multivariate discriminant model differentiated healthy samples and glaucomatous samples with good accuracy [healthy 89.5% and glaucomatous 97.6% for the same breed (Basset Hounds); and healthy 85.0% and glaucomatous 85.5% for different breeds (Beagles versus Basset Hounds)]. Raman spectroscopic screening can be used for *in vitro* detection of glaucomatous changes in retinal tissue with a high specificity. © 2011 Society of Photo-Optical Instrumentation Engineers (SPIE). [DOI: 10.1117/1.3642010]

Keywords: glaucoma; raman spectroscopy; retinal ganglion cells; detection; support vector machine.

Paper 11126R received Mar. 16, 2011; revised manuscript received Aug. 4, 2011; accepted for publication Sep. 1, 2011; published online Oct. 13, 2011.

## 1 Introduction

Glaucoma is an optic neuropathy which is characterized by a progressive optic nerve head cupping and ultimately vision loss. It is the second leading cause of blindness worldwide according to the World Health Organization.<sup>1</sup> Glaucoma is characterized by a progressive death of retinal ganglion cells (RGCs), which ultimately results in the loss of visual function. Elevated intraocular pressure (IOP) is considered a primary risk factor for the progression of glaucomatous neuropathy.<sup>1,2</sup> In many patients, despite the adequate control of the IOP, the loss of vision continues to progress, which necessitates further identification of molecular mechanisms responsible for the glaucomatous neurodegeneration and development of novel diagnostic modalities, which can detect glaucomatous changes even in patients where IOP is considered normal.<sup>2-5</sup>

Raman spectroscopy is a technique that provides rapid characterization of tissue and bodily fluids in a nondestructive and noninvasive fashion. This methodology relies on inelastic scattering of monochromatic light by macromolecules in the tissue, usually from a laser in the visible or near-infrared range.<sup>6</sup> Raman spectroscopy is one of the ideal tools to obtain the general biochemical landscape of biological samples. In recent years a marked upsurge in the use of Raman spectroscopy as a noninvasive probing technique has occurred in biomedical research.

The diverse applications have included characterization of different cancers by obtaining biochemical information from an *in situ* sample such as lung cancer,<sup>7-9</sup> vitamin distribution in tissues<sup>10,11</sup> and the investigation of bone properties.<sup>12</sup> Once the Raman spectra of a tissue sample are acquired, mathematical classification techniques are utilized to differentiate the spectral signatures of diseased and normal tissues.

In order to better understand glaucomatous changes that occur in the retina and optic nerve and develop effective diagnostic and therapeutic modalities for human disease, it is essential to use animal models that recapitulate the silent and slow development of the disease characterized by a progressive loss of a RGC function. Numerous inducible animal models of glaucoma have been used successfully to test different therapeutic strategies and to evaluate molecular mechanisms of RGC damage resulting from chronic elevation of IOP.<sup>2,13,14</sup> Due to the similar size to the human eye, spontaneously occurring large animal models (hereditary canine glaucoma) offer a unique opportunity to obtain functional, structural, and molecular data using instrumentation identical to that used in human patients.<sup>15</sup>

The primary purpose of this study was to explore the potential of using Raman spectroscopy for characterization of glaucomatous molecular signatures. We compared the Raman spectral differences between canine glaucomatous eyes and healthy (control) eyes. The overall objective was to identify spectroscopic markers associated with glaucomatous changes

Address all correspondence to: Chenxu Yu, Iowa State University, Agricultural and Biosystems Engineering, 3224 NSRIC, Ames, Iowa 50011; Tel: 5152944554; Fax: 5152944250; E-mail: chenxuyu@iastate.edu.

in retinal ganglion cells, and to develop a classification methodology which potentially could be effectively used to develop *in vivo* imaging modalities for early glaucoma detection using Raman spectroscopy.

## 2 Materials and Methods

### 2.1 Animals and Tissue Collection

All animal studies were conducted in accordance with the ARVO Statement for Use of Animals in Ophthalmic and Vision Research, and procedures were approved by the Iowa State University Committee on Animal Care (IACUC Grant Nos. 11-09-6827-K and 9-05-5968-K). Eyes were collected from eight Basset Hounds with hereditary progressive angle closure glaucoma from our colony,<sup>15</sup> and retinal sections were used for Raman spectroscopic investigation. Additionally, eyes from 12 adult healthy Beagles and 3 healthy Basset Hounds were used to serve as a control tissue. All control animals underwent ocular examination (slit lamp biomicroscopy, intraocular pressure evaluation, indirect ophthalmoscopy, gonioscopy), to rule out the possible presence of ocular disease before inclusion in the study.

Eyes were surgically removed from glaucomatous Basset Hounds once their IOP reached the 35 to 45 mmHg range. At the time of removal, eyes did not have vision, but had positive photopic blink response and pupil light reflex responses. Eyes from control healthy Beagles and healthy Basset Hounds were collected after euthanasia for reasons not related to this study. Eyes were fixed in the 10% buffered paraformaldehyde for 24 h and then rinsed and paraffin imbedded. Twenty micrometer thick central retinal sections containing optic nerve head profile were made and placed on gold-aluminum coated histology slides for the purposes of Raman imaging. Raman spectra were acquired from the fixed tissue sections using a Raman microscope with 4×, 10×, and 100× objectives.

### 3 Acquisition of Raman Spectrum from Retinal Tissues

Raman measurements were performed using a DXR Dispersive Raman Microscope (Thermo Scientific, Inc., Madison, Wisconsin) with 780 nm, 14 mW excitation laser with 50 μm pinhole at ambient temperature. Raman spectra were collected with various exposure times (15, 20, 30, 60, 99 s) from 550 and to 2000 cm<sup>-1</sup> at a resolution of 1 cm<sup>-1</sup>.

With the 100× objective, individual RGCs can be resolved at subcellular spatial resolution (1 to 1.5 μm), and potential characterization of spectroscopic subcellular compartmentation within individual RGC can be achieved. However, this study focused on differentiation of healthy and glaucomatous tissues as whole units, and subcellular compartmentation was not investigated. Five spectra were collected from each individual cell at different spots and an average spectrum was then calculated (to minimize the variation due to subcellular compartmentation) for that cell to be used as one RGC spectrum in subsequent analysis (105 RGC spectra from glaucomatous Basset Hound tissues, 105 RGC spectra from healthy Basset Hound tissues, and 162 RGC spectra from healthy Beagle tissues, respectively). With 4× and 10× objectives, spectra were collected from the entire RGC region as a whole (215 spectra from glaucomatous Basset Hound tissues, 220 spectra from healthy Basset Hound tissues,

and 205 spectra from healthy Beagle tissues, respectively). The intensity of the Raman spectrum acquired with low magnification objectives (4× and 10×) was stronger than that of an individual RGC cell due to the larger amount of Raman photons being collected. Nonetheless, their spectroscopic characteristics (i.e., peak wave numbers and peak profiles) were almost identical. Lower magnification objectives delivered the laser power to a much larger area on the tissue samples (~1 mm<sup>2</sup> at 4×), and resulted in a much smaller laser energy density at the tissue surface. After normalization, all spectra from the same type of samples were pooled together for the development and testing of the discriminant model generated using a support vector machine (SVM). The total spectra for each type of samples were: 320 from glaucomatous Basset Hound tissues, 325 from healthy Basset Hound tissues, and 367 from healthy Beagle tissues.

### 4 Spectral Data Processing

All spectra were baseline corrected and smoothed using a 20-point averaging algorithm to reduce the baseline variability and background noises at the region between 550 and 2000 cm<sup>-1</sup>. All spectra were then normalized by setting the intensity of the strongest Raman peak (amide I) to unity. All data processing was conducted using Omnic professional Software Suite (Thermo Scientific, Inc., Madison, Wisconsin).

A standardized residual spectrum (SRS) was then calculated from the original spectral data using Eq. (1).

$$\text{SRS}(\text{Raman shift}) = \frac{X(\text{Raman shift}) - \bar{X}(\text{Raman shift})}{s.d.(\text{Raman shift})}, \quad (1)$$

where SRS is the standardized residual spectral intensity at each Raman shift wavenumber,  $X$  is the Raman intensity of each individual spectrum at the same Raman shift,  $\bar{X}$  is the mean Raman intensity of all spectra from the same data set (i.e., diseased or control) at the same Raman shift, and  $s.d.$  is the standard deviation of the Raman intensity within the data set at the same Raman shift. The SRS highlights the variations in spectral data measured from the same type of samples (i.e., control versus diseased), and they were used in a subsequent discriminant analysis.

It should be noted that the chemical fixation with paraformaldehyde alters the chemical makeup of the tissues and changes the Raman spectroscopic characteristics of the tissue samples. However, it has been demonstrated that fixation with paraformaldehyde produces spectral content that is closest to that of living cells.<sup>16</sup> Using hierarchical cluster analysis and principal components analysis (PCA) on individual Raman spectra randomly selected from the nuclear regions of single cancer cells, Draux and co-workers have shown that formalin-fixation and cytocentrifugation are sample preparation methods that have little impact on the biochemical information as compared to living conditions.<sup>17</sup> Although the chemical fixation is a possible confounding variable in the differentiation and classification analysis of the spectra acquired from the normal and diseased eye samples, its impact on the analysis is limited in nature since all samples were processed under identical conditions.

### 5 PCA and Data Compression for SVM Discriminant Modeling

For discriminant analysis, as the dimensions of the data set (i.e., each wave number in the spectral data represents an

independent dimension) become large, the limitation on the capability of detecting distinguishable classes becomes severe.<sup>18</sup> PCA was used in this study for the dimensionality reduction. The data sets (SRS) were compressed into PC scores, and 10 to 50 PC scores (accounted for 94% to 99% of the total variance in the data sets, as shown in Fig. 6) were selected from 1506 dimensional hyperspectral data as inputs for multivariate discriminant classification model generated using a Support Vector Machine (Ref. 19) implemented with MATLAB SVM toolbox (The Mathworks, Inc., Natick, Massachusetts) using polynomial kernel function.<sup>20</sup> Training sets (110 spectra from each group, 330 in total) and testing sets (100 spectra/tests) were randomly chosen from the measured spectra [from glaucomatous Basset Hounds (diseased), healthy Basset Hounds (control 1), and healthy Beagles (control 2)]. Average classification accuracy was calculated from 10 random replications of the discriminant process.

## 6 Results

### 6.1 Spectroscopic Characterization of Retinal Ganglion Cells from the Retinal Tissues

The optical images of the retinal tissue sections of glaucomatous Basset Hound, healthy Hasset Hound, and healthy Beagle are shown in Fig. 1. The layers of RGCs were identified under the microscope, as shown in the figures.

Raman peaks are represented by their wave number (Raman shift) and intensity. The peak intensities are dependent on many factors that may vary from sample to sample (i.e., sample size, exposure time, etc.), but their Raman shift remains identical as long as the molecular makeup is the same. A typical Raman spectra and SRS measured from glaucomatous Basset Hound RGCs are shown in Fig. 2 in the 550 to 2000  $\text{cm}^{-1}$  range. From the spectra, we could identify contributions from functional groups of the major macromolecules presented in the cells. Proteins (i.e., amide I and III peaks, phenylalanine peaks, tryptophan peaks, tyrosine peaks) and DNAs (i.e., adenine peak, thymine peaks) can both be characterized with specific Raman bands. The differences shown by these Raman signature bands can be used to differentiate diseased tissues from healthy ones.

To compare the biochemical changes between RGCs of glaucomatous Basset Hounds and healthy dogs (Beagles and Basset Hounds), represented by their Raman spectroscopic signatures, we measured Raman spectra from 105 RGCs from 8 glaucomatous Basset Hounds, 105 RGCs from 3 healthy Basset Hounds, and 162 RGCs from 12 healthy Beagles with normal vision.

The average and difference spectra between healthy and glaucomatous dogs are shown in Fig. 3. The difference spectrum was acquired by subtracting the control (healthy Beagle and healthy Basset Hound) from the diseased (glaucomatous Basset Hound) spectra, respectively. The wave number and intensity changes in those Raman bands of biological importance were indicative of changes in the secondary structure and variations in local environments of intracellular proteins as well as DNAs, which may determine the characteristics of glaucomatous tissues. Differences at amide III peaks illustrate the changes in the overall concentration of total proteins,<sup>21</sup> the composition of proteins also shows some significant differences, as evidenced by Raman bands of various amino acids, at 800 to 1200  $\text{cm}^{-1}$ . These changes can potentially be used as spectroscopic markers for the detection of glaucoma.

## 7 Discriminant Classification of Glaucomatous Versus Healthy Spectra Using Support Vector Machine

A SVM was utilized to generate discriminant classification models to classify a measured spectrum from a retinal tissue sample into the two categories (glaucomatous and normal). One hundred and ten spectra measured from the control group (healthy Beagles and healthy Basset Hounds) and 110 spectra measured from the glaucomatous group (glaucomatous Basset Hounds) were used as the training data sets to create the SVM discriminant models. After compressing the original spectral data using PCA, the resulted PC scores were used to calculate hyperdimensional classifier. The classification model generated with 10 PC scores (10 D hyperdimensional classifier) is illustrated in Fig. 4. The support vectors defined a hyperplane that divided the 10 D hyperspace into two domains: normal and glaucomatous. The classification model was then validated through random testing of 10 testing data sets, each containing 100 spectra measured from the control and glaucomatous retinal tissues, respectively. The average classification accuracy was then calculated to evaluate the performance of the classification models.

## 8 Effect of Spectral Data Processing for the Classification Accuracy

Using PCA, the dimensionality of the spectral data was greatly reduced. With 50 PCs, over 99% of the total variance within spectral data measured for each type of sample could be explained. Ten PCs accounted for 94% of the total variance for each type of samples. Figure 5 shows the impact of the number

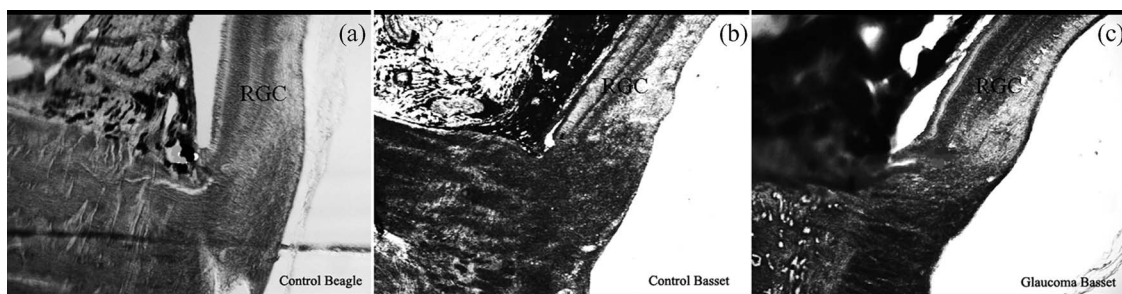


**Fig. 1** Optic images of retinal tissue sections from a healthy Beagle (a), a healthy Basset Hound (b), and glaucomatous Basset Hounds (c) on gold coated slides (RGC—retinal ganglion cell layer).

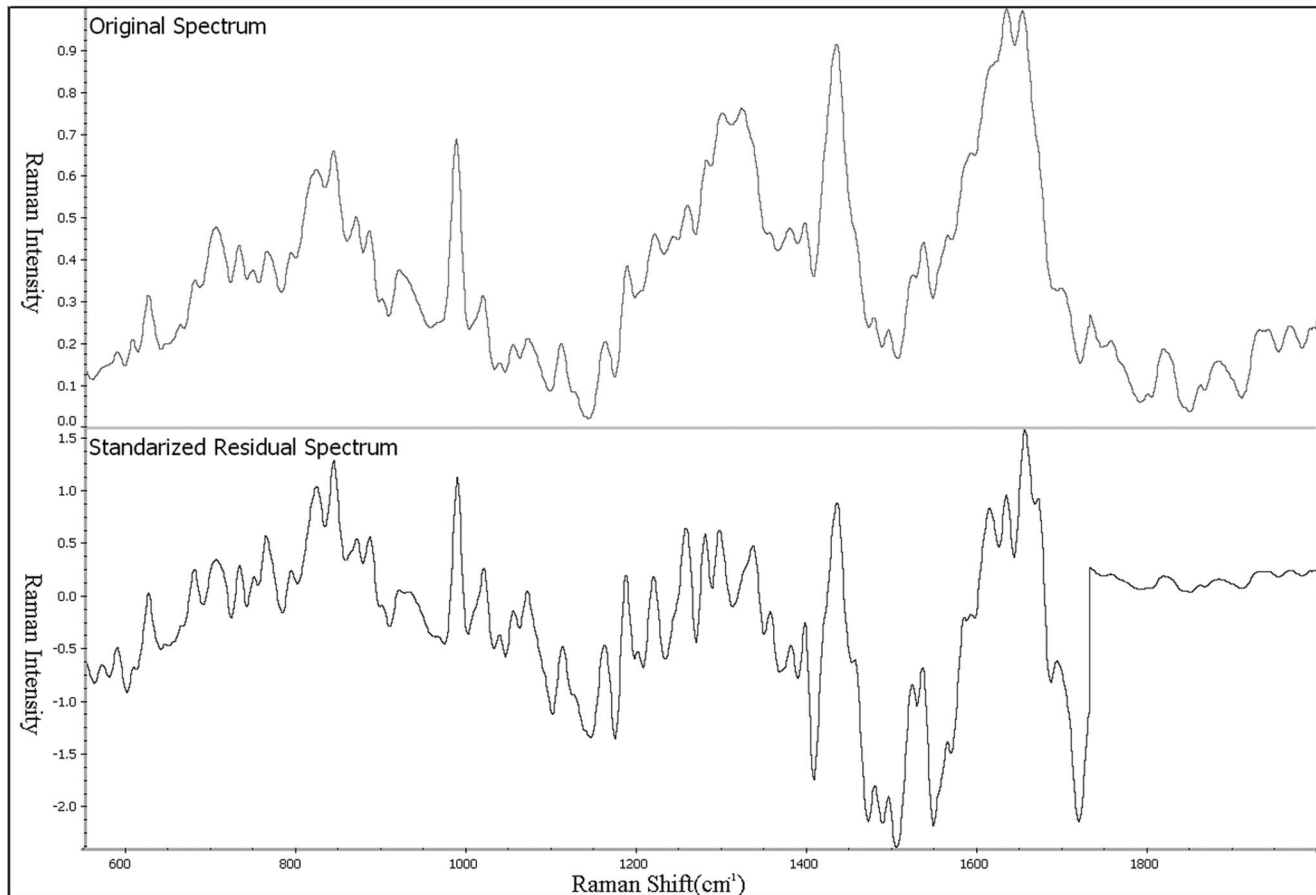


Fig. 2 Typical Raman spectrum and SRS of RGCs from glaucomatous Basset Hounds.

of PCs used in the SVM discriminant model on the classification accuracy for healthy Basset Hounds (control) and glaucomatous Basset Hounds (diseased). Consistently, classification accuracy for glaucomatous RGCs was better than that for normal RGCs. We hypothesize that biochemical changes caused by glaucoma may introduce characteristic spectroscopic signatures that lead to more coherently intercorrelated clustering of the data representing glaucomatous RGCs in the hyperspace of the SVM classifier, which results in the better classification accuracy.

As the number of PCs increased from 10 to 30, the classification accuracy for a glaucomatous Basset Hound reached 100%. Since the number of spectra used in training the discriminant model (220) is far larger than the number of PC scores (<50), it is reasonable to believe that the high classification accuracy is not caused by overfitting.<sup>22</sup> Given the fact that the glaucomatous Basset Hounds investigated in this study were at the late stage of the disease and have lost almost 100% vision loss, it could be reasoned that severe physiological changes have occurred in their RGCs, which may result from significant biochemical alterations to the cells that are captured in their Raman spectral data. Interestingly, the classification accuracy for healthy Basset Hounds peaked at 30 PCs (~91%) and slightly declined with more PCs being used in the discriminant model, suggesting that further optimization is possible by identifying the PCs that are the most responsible for differentiating the diseased group from the healthy group.

## 9 Classification Differences between Different Breeds of Dogs

Hereditary glaucoma is a genetic disorder affecting RGCs. It is reasonable to hypothesize that the biochemical makeup of the RGCs in diseased Basset Hounds differs from that of healthy Basset Hounds. As demonstrated by the high accuracy of the classification results reported before, these intrinsic biochemical differences were captured by their Raman spectroscopic characteristics.

We have previously demonstrated that the gene and protein expression in the retina of glaucomatous and healthy dogs are not breed related, but it rather depends on the stage of glaucoma.<sup>23</sup> Therefore, a valid question to ask is whether or not the spectroscopic differences between healthy and glaucomatous retinal tissue exist regardless of the breeds of the dogs. To answer this question, we have compared Raman spectroscopic data between spectral specimens of two healthy control populations (healthy Basset Hounds and healthy Beagles).

The classification results to differentiate glaucomatous Basset Hounds and healthy Beagles are shown in Fig. 6 and Table 1. A slight reduction in classification accuracy was observed. With 10 PCs, 85.0% of RGCs were correctly classified for the healthy (control) group, and 85.5% RGCs were correctly classified for the glaucomatous group. When classification accuracy was compared within the same breed (control healthy Basset Hounds and glaucomatous Basset Hounds), 89.5%

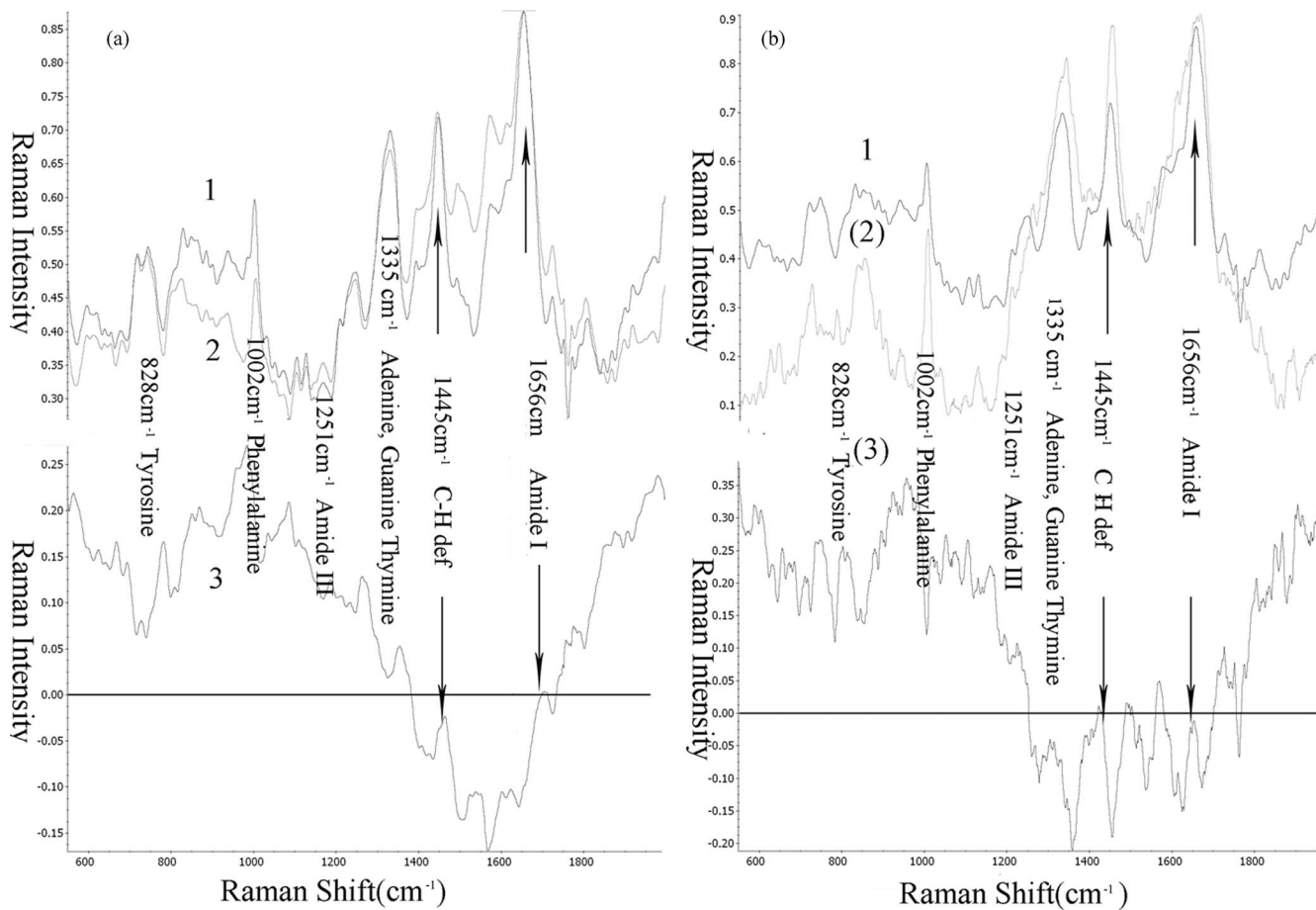


**Fig. 3** Average Raman spectra and Difference spectra between glaucomatous and normal RGCs: (a) Healthy Basset Hounds versus glaucomatous Basset Hounds; (b) Healthy Beagles versus glaucomatous Basset Hounds. 1. Glaucomatous Basset Hound; 2. Healthy Basset Hound; 3. Difference spectrum (2). Healthy Beagle; (3). Difference spectrum.

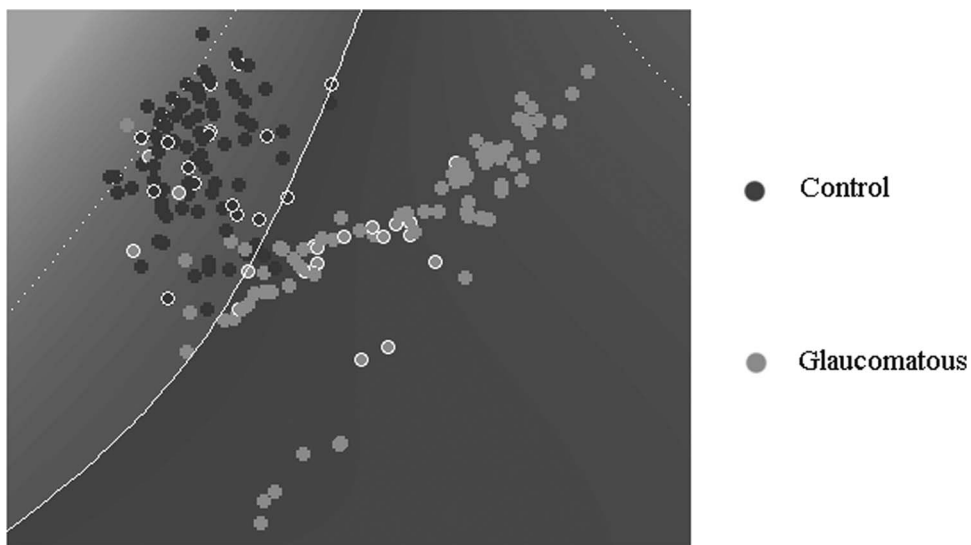


**Fig. 4** An example of the trained classifier by the support vector machine. The trained classifier between the spectra from RGCs from control healthy Basset Hounds (black) and glaucomatous Basset Hounds (gray) is shown. It should be noticed that this is a two-dimensional projection of a 10-D hyperplane separation, thus some overlapping was observed between the two groups while in 10-D space they were well separated. The SVM separating function divided the space into two areas represented by different colors (black and gray). The “circled” dots are support vectors.

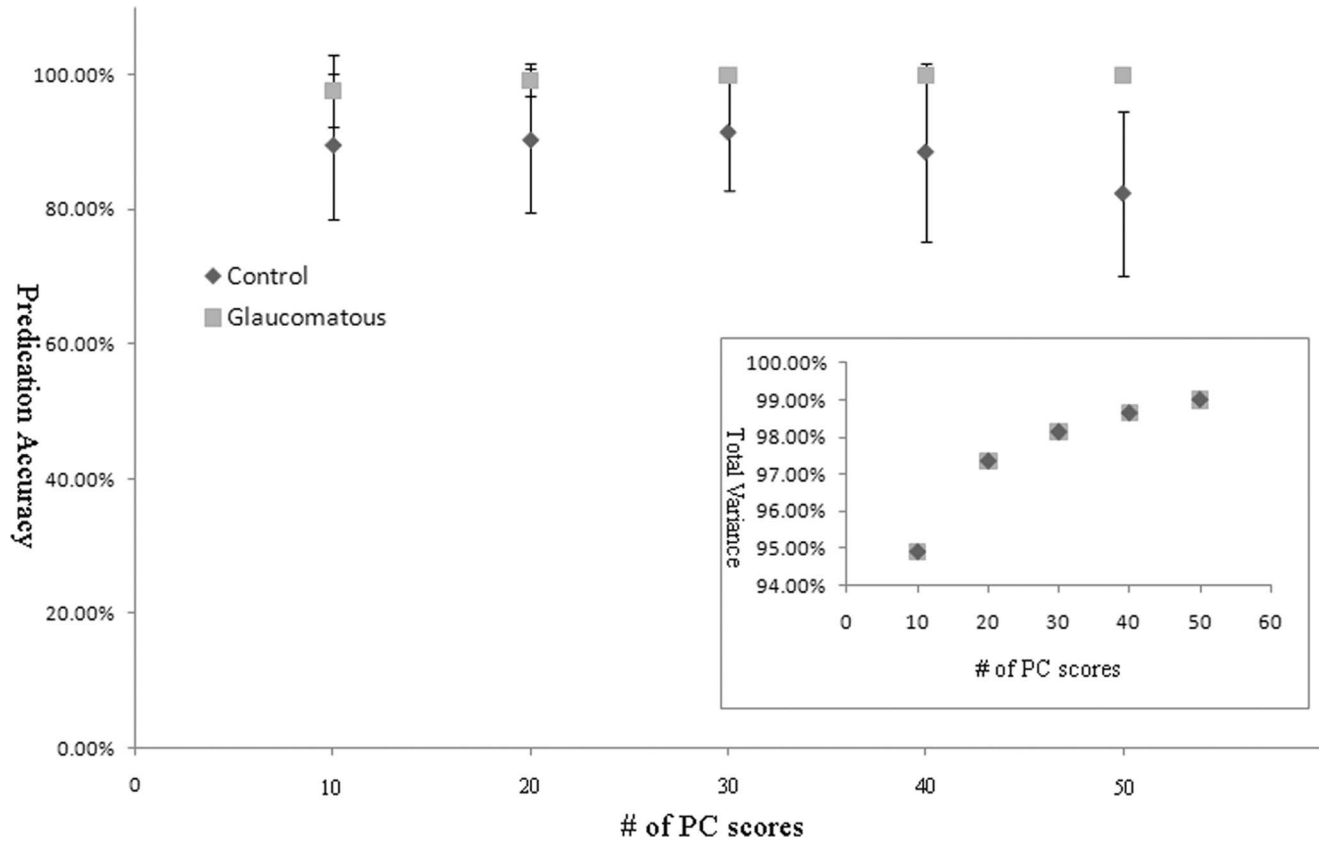


**Fig. 5** The influence of the number of PC scores used in SVM discriminant models on the differentiation accuracy of classifying tissues into healthy and glaucomatous categories. Each error bar indicates the standard deviation of classification accuracy from 10 replications of different training and testing data sets. The inlet shows the total variance accounted for by the number of different PC scores.

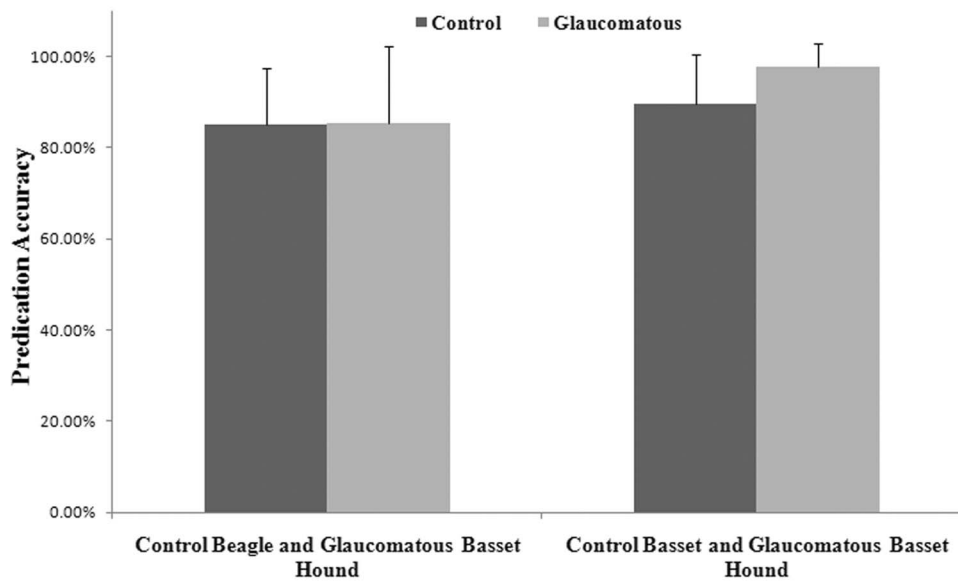


**Fig. 6** Classification performance of the SVM model to differentiate healthy tissues from glaucomatous tissues. Each error bar indicates the standard deviation of classification accuracy from 10 replications with different training and testing data sets.

**Table 1** The average classification accuracies for retinal ganglion cells between control and diseased tissues using 10 PCs in SVM discriminant analysis.

	Healthy Basset Hounds versus glaucomatous Basset Hounds		Healthy Beagle versus glaucomatous Basset Hounds	
	Normal RGCs	Glaucomatous RGCs	Normal RGCs	Glaucomatous RGCs
Classified as Normal	89.5%	97.6%	85.0%	85.5%
Classified as Glaucomatous	10.5%	2.4%	15%	14.5%

RGCs were correctly classified for the healthy group, and 97.6% were correctly classified for the glaucomatous group.

These results strongly suggest that there are significant biochemical differences between the retinal ganglion cells of glaucomatous and healthy dogs that can be identified from their Raman spectra, even between different breeds of dogs. The slight reduction in classification accuracy between different breeds may be related to the interbreed genetic discrepancy, which may result in a greater spread of the data points, and may lead to the mild reduction in the classification accuracy.

The hereditary glaucoma in Basset Hounds is most likely a result of genetic mutation(s) in the ocular tissues, and potentially all cells in the body. The classification results using the Raman spectra of fibroblast cells and retinal ganglion cells extracted from the control (healthy Beagles) and glaucomatous animals (Basset Hounds) are shown in Fig. 7 and Table 2. A dramatic reduction in classification accuracy was observed. Only 69.2% of fibroblasts were correctly classified for the healthy group, and only 46% of fibroblasts were correctly classified for the glaucomatous group. These observations suggested that the spectroscopic differences between healthy and glaucomatous animals are probably tissue type specific: they could only be observed with high certainty in RGCs, but not in fibroblast cells. The possible explanation for observed changes is that the biochemical footprints associated with glaucoma could be the result of the possible genetic abnormality resulting in a disease phenotype only in ocular tissues. However, it cannot be excluded that the presence of more aggressive disease phenotype in affected eyes (elevated intraocular pressure, neuroinflammatory changes, neuronal death, etc.) resulted in more prominent biochemical changes providing a distinct spectroscopic pattern.

## 10 Discussion

Glaucoma is a disease which affects millions of patients worldwide, and frequently is diagnosed only when significant optic nerve damage has already developed. For the purposes of this study we have intentionally used tissues from animals with the advanced hereditary glaucoma to make sure that observed spectroscopic changes present in glaucomatous eyes can be detected. For this technology to become a viable clinical tool, it is obvious that testing needs to be done in animals at a very early stage of the disease, which would be more representative of the condition seen in early glaucoma human patients and glaucoma disease suspects who are in the strongest need of accurate and early diagnosis.

In this study, support vector machine discriminant classification modeling was incorporated with Raman spectroscopy to differentiate and classify differences between glaucomatous and healthy (control) RGCs. It was demonstrated that Raman imaging of RGC chemical profiles results in the high recognition accuracy of the tissue status (91% of healthy RGCs and 100% of glaucomatous RGCs were classified correctly by a predictive model which was trained using defined glaucomatous and healthy control samples). Furthermore, Raman spectroscopic signatures associated with changes in intracellular protein compositions were identified, which potentially can be used as spectroscopic biomarkers for glaucoma diagnosis *in vivo* in the future. To date, Raman spectroscopy has not been fully explored to detect molecular changes in eye tissues associated with glaucoma.

For the 780 nm diode laser that was used in this study, the threshold limit value (TLV) can be calculated as follows,<sup>24,25</sup> where CA is the correction factor for different wavelength:

$$TLV = 1.8 \times 10^{0.002 \times (\lambda - 700)} \times t^{-1/4} \text{ mw/cm}^2. \quad (2)$$

The TLV determines the maximum permissible energy exposure to the retina in an *in vivo* measurement. In the current study, with 15 and 99 s exposure time, the TLV is 1.32 and 0.82 mW/cm<sup>2</sup>, respectively. The laser spot-size on the sample was ~1 mm<sup>2</sup> with 4× objective, and ~10% laser power (1.4 mW) was delivered on the sample. The resulting power density on the sample was 140 mW/cm<sup>2</sup>, significantly higher than the TLV. To utilize Raman spectroscopy for *in vivo* imaging, the laser power density on the retina has to be greatly reduced.

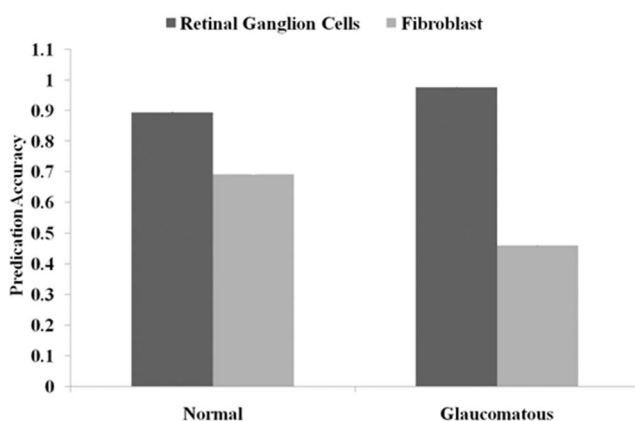


**Fig. 7** Classification accuracy for RGCs and fibroblast cells from glaucomatous Basset Hounds (glaucomatous) and healthy Beagles (normal).

**Table 2** The average classification accuracies for retinal ganglion cells and fibroblast cells between normal Beagle and glaucomatous Basset Hounds using 10 PCs in SVM discriminant analysis.

	RGCs		Skin fibroblasts	
	Normal (Beagles)	Glaucomatous (Basset Hounds)	Normal (Beagles)	Glaucomatous (Basset Hounds)
Classified as Normal	85.0%	85.5%	69.2%	54.0%
Classified as Glaucomatous	15.0%	14.5%	30.8%	46.0%

Raman scattering is a weak phenomenon in comparison to autofluorescence coming mostly from protein molecules,<sup>26</sup> Raman spectral fingerprints can be overwhelmed by stronger fluorescence background when *in vivo* imaging is conducted. Earlier reports utilizing Raman spectroscopy for ophthalmological investigation focused on detection of human macular pigment and glutamate in the eyes, in which the excitation laser wavelength was selected to resonate with the vibrational modes of the pigment/glutamate molecules, and an enhanced Raman signal was achieved.<sup>25,27</sup> To acquire a Raman signal directly from the RGC cells without the resonance enhancement effects, the autofluorescence background has to be removed before the analysis of the vibrational bands takes place. The most common methods for background removal, as the one currently used in this study, are based on digital signal subtraction utilizing the common feature of fluorescent backgrounds—a smooth function of the emission wavelength.<sup>28,29</sup> Assuming the fluorescence signal contributes  $F$  photons to the recorded signal, while Raman signal adds an additional  $R$  photons (for a typical experimental setting  $R \ll F$ ), the shot noise introduced by the signal in this case was calculated as  $N = (F + R)^{1/2} \approx F^{1/2}$ , resulting in a signal-to-noise ratio (SNR) equal to  $R/F^{1/2}$  after the fluorescent background has been digitally subtracted from the data. This level of noise is still worse than the ideal SNR in the absence of the fluorescent background, which can be defined as  $SNR_{ideal} = R^{1/2}$ . From the above equations, it is evident that the SNR degrades by a factor of  $(F/R)^{1/2}$ , and in order to compensate for it, the data acquisition times of roughly equal to or longer than  $F/R$  are required. In other words, if the fluorescent background is somehow reduced by a factor of 1000, the acquisition times to achieve the same SNR Raman spectra should also be cut by approximately a factor of 1000 (assuming that the shot noise is a predominant source of the data noise). If the acquisition time (exposure time) can be significantly reduced, the higher laser power can be potentially used to obtain a higher-quality spectral signal without reaching the safety limit.

One possible solution to overcome excessive retinal exposure to the high levels of laser energy is to utilize pulse laser with extreme short time-gated detection ( $10^{-12}$  s). With such short exposure and detection time, background fluorescence is eliminated (shorter than the fluorescence lifetime so that fluorescence is not developed), and the signal-to-noise ratio of the Raman spectral measurement can be significantly improved, allowing much weaker Raman signals to be detectable.<sup>30,31</sup> An extremely short detection time also allows a much higher laser power to be applied without increasing the overall retinal laser energy exposure. Simple calculation reveals that at  $10^{-12}$  exposure time, the TLV is  $2601 \text{ mW/cm}^2$ , which is much higher compared to the energy levels used in this study.

In this study, we have demonstrated that Raman imaging can be effectively used for the classification of neuronal changes associated with glaucoma. Further refinement of Raman imaging instrumentation and detection algorithms may provide an exciting opportunity for development of the novel and sensitive diagnostic modalities for the early detection of glaucoma.

### Acknowledgments

This study has been supported by the U.S. Department of Veterans Affairs Center for Prevention and Treatment of Visual Loss.

### References

- H. A. Quigley, "Neuronal death in glaucoma," *Prog. Retin Eye Res.* **18**, 39–57 (1999).
- J. C. Morrison, "Elevated intraocular pressure and optic nerve injury models in the rat," *J. Glaucoma* **14**, 315–317 (2005).
- L. A. Levin, "Direct and indirect approaches to neuroprotective therapy of glaucomatous optic neuropathy 1," *Surv. Ophthalmol.* **43**, S98–S101 (1999).
- N. Osborne, G. Chidlow, M. Nash, and J. Wood, "The potential of neuroprotection in glaucoma treatment," *Curr. Opin. Ophthalmology* **10**, 82–92 (1999).
- J. M. Tielsch, A. Sommer, J. Katz, R. Royall, H. Quigley, and J. Javitt, "Racial variations in the prevalence of primary open-angle glaucoma: the Baltimore Eye Survey," *Jama* **266**, 369–374 (1991).
- D. Long, *Raman Spectroscopy*, McGraw-Hill, New York (1977).
- Z. Huang, A. McWilliams, H. Lui, D. McLean, S. Lam, and H. Zeng, "Near infrared Raman spectroscopy for optical diagnosis of lung cancer," *Int. J. Cancer* **107**, 1047–1052 (2003).
- Z. Huang, H. Lui, D. McLean, M. Korbelik, and H. Zeng, "Raman spectroscopy in combination with background near-infrared autofluorescence enhances the *in vivo* assessment of malignant tissues," *Photochem. Photobiol.* **81**, 1219–1226 (2005).
- A. Taleb, J. Diamond, J. McGarvey, J. Beattie, C. Toland, and P. Hamilton, "Raman microscopy for the chemometric analysis of tumor cells," *J. Phys. Chem. B* **110**, 19625–19631 (2006).
- J. R. Beattie, C. Maguire, S. Gilchrist, L. J. Barrett, C. E. Cross, F. Possmayer, M. Ennis, J. S. Elborn, W. J. Curry, J. J. McGarvey, and B. C. Schock, "The use of Raman microscopy to determine and localize vitamin E in biological samples," *FASEB J.* **21**, 766–776 (2007).
- P. Pudney, M. Mélot, P. Caspers, A. Van Der Pol, and G. Puppels, "An In Vivo Confocal Raman Study of the Delivery of Trans Retinol to the Skin," *Appl. Spectrosc.* **61**, 804–811 (2007).
- A. Carden, R. Rajachar, M. Morris, and D. Kohn, "Ultrastructural changes accompanying the mechanical deformation of bone tissue: a Raman imaging study," *Calcif. Tissue Int.* **72**, 166–175 (2003).
- C. A. Rasmussen and P. Kaufman, "Primate glaucoma models," *J. Glaucoma* **14**, 311–314 (2005).
- H. Levkovitch-Verbin, "Animal models of optic nerve diseases," *Eye* **18**, 1066–1074 (2004).
- S. D. Grozdanic, H. Kecova, M. Harper, W. Nilaweera, M. Kuehn, and R. Kardon, "Functional and structural changes in a canine model of

- hereditary primary angle-closure glaucoma," *Invest. Ophthalmol. Visual Sci.* **51**, 255–263 (2010).
16. A. D. Meade, C. Clarke, F. Draux, G. D. Sockalingum, M. Manfait, F. M. Lyng, and H. J. Byrne, "Studies of chemical fixation effects in human cell lines using Raman microspectroscopy," *Anal. Bioanal. Chem.* **396**, 1781–1791 (2010).
  17. F. Draux, C. Gobinet, J. Sulé-Suso, A. Trussardi, M. Manfait, P. Jeannesson, and G. D. Sockalingum, "Raman spectral imaging of single cancer cells: probing the impact of sample fixation methods," *Anal. Bioanal. Chem.* **397**, 2727–2737 (2010).
  18. L. Jimenez and D. Landgrebe, "Supervised classification in high-dimensional space: geometrical, statistical, and asymptotical properties of multivariate data," *IEEE Trans. Syst. Man Cybern., Part C Appl. Rev.* **28**, 39–54 (2002).
  19. I. Steinwart and A. Christmann, *Support Vector Machines*, Hoboken, Secaucus, NJ (2008).
  20. S. Gunn, "Support vector machines for classification and regression," *ISIS Technical Report*, p. 14 (1998).
  21. A. Herrero, "Raman spectroscopy for monitoring protein structure in muscle food systems," *Crit. Rev. Food Sci. Nutr.* **48**, 512–523 (2008).
  22. E. K. Kemsley, *Discriminant Analysis and Class Modeling of Spectroscopic Data*, John Wiley & Sons, Ltd., Hoboken, NJ (1998).
  23. B. Jiang, M. M. Harper, H. Kecova, G. Adamus, R. H. Kardon, S. D. Grozdanic, and M. H. Kuehn, "Neuroinflammation in advanced canine glaucoma," *Mol. Vis.* **16**, 2092–2108 (2010).
  24. J. S. Myers, M. G. Trevisani, N. Imami, L. W. Herndon, M. L. Wolbarsht, R. R. Allingham, K. D. Straub, and M. B. Shields, "Laser energy reaching the posterior pole during transscleral cyclophotocoagulation," *Arch. Ophthalmol.* **116**, 488–491 (1998).
  25. A. Katz, E. Kruger, G. Minko, C. Liu, R. Rosen, and R. Alfano, "Detection of glutamate in the eye by Raman spectroscopy," *Proc. SPIE* **4098**, 169–171 (2000).
  26. A. Barth and C. Zscherp, "What vibrations tell about proteins," *Q. Rev. Biophys.* **35**, 369–430 (2002).
  27. R. J. Erckens, F. Jongsma, J. Wicksted, F. Hendrikse, W. March, and M. Motamedi, "Raman spectroscopy in ophthalmology: from experimental tool to applications in vivo," *Lasers Med. Sci.* **16**, 236–252 (2001).
  28. G. Schulze, A. Jirasek, M. Yu, A. Lim, R. Turner, and M. Blades, "Investigation of selected baseline removal techniques as candidates for automated implementation," *Appl. Spectrosc.* **59**, 545–574 (2005).
  29. C. A. Lieber and A. Mahadevan-Jansen, "Automated method for subtraction of fluorescence from biological Raman spectra," *Appl. Spectrosc.* **57**, 1363–1367 (2003).
  30. T. Tahara and H. Hamaguchi, "Picosecond Raman spectroscopy using a streak camera," *Appl. Spectrosc.* **47**, 391–398 (1993).
  31. P. Matousek, M. Towrie, A. Stanley, and A. Parker, "Efficient rejection of fluorescence from Raman spectra using picosecond Kerr gating," *Appl. Spectrosc.* **53**, 1485–1489 (1999).